Numerical simulation of double-diffusive Marangoni convection

T. L. Bergman

Citation: Physics of Fluids **29**, 2103 (1986); doi: 10.1063/1.865597
View online: http://dx.doi.org/10.1063/1.865597
View Table of Contents: http://scitation.aip.org/content/aip/journal/pof1/29/7?ver=pdfcov
Published by the AIP Publishing

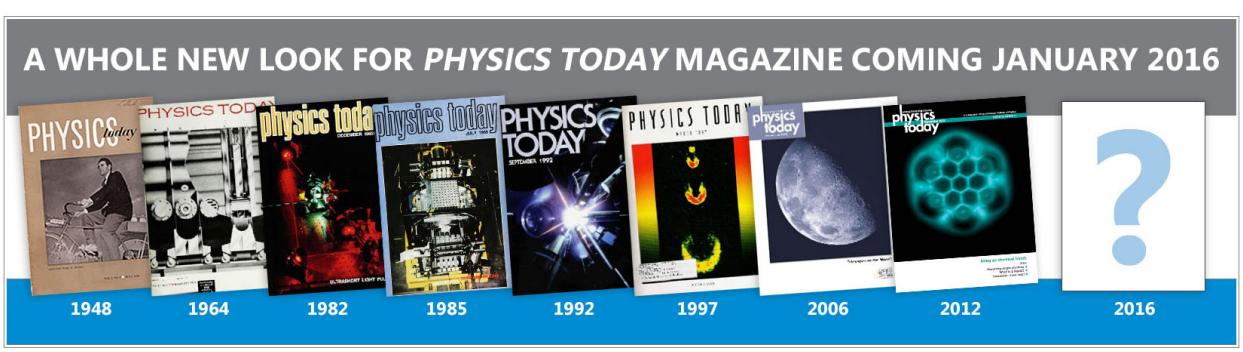

Numerical simulation of double-diffusive Marangoni convection

T. L. Bergman
Department of Mechanical Engineering, The University of Texas at Austin, Austin, Texas 78712

(Received 29 January 1986; accepted 11 April 1986)

Marangoni convection is important in a variety of physical systems and occurs as a result of surface tension gradients at a liquid free surface. In general, liquid surface tension varies with temperature and species concentration in a binary fluid. If the temperature and concentration distributions make opposing contributions to the overall surface tension gradient at a free surface, convective motion, as well as heat and mass transfer within the system, is shown to depend on double-diffusive effects. This situation is analogous to double-diffusive natural convection, in that convection may occur, even though the overall surface tension difference along the free surface suggests stagnant fluid conditions.

I. INTRODUCTION

It is well known that buoyancy forces can induce motion in liquids contained in enclosures with, for example, differentially heated end walls.[1,2] However, when a free surface is present, variations in the liquid surface tension, as a result of thermal gradients along the free surface, can also induce fluid motion.[3]

The density and surface tension may also vary with the local species concentration in a binary fluid. As such, buoyancy or surface-tension-driven convection may be induced by species concentration gradients in binary fluids contained, for example, within an enclosure whose end walls are maintained at different concentrations.[4]

Recently, considerable progress has been made in developing an understanding of natural convection in double-diffusive systems such as salt-stratified fluid layers heated from below.[2,5] In these systems, the fluid density depends on local temperatures and concentrations. When the temperature and concentration distributions make opposing contributions to the vertical density gradient, and when the Lewis number is not unity, diffusional processes can induce convective motion even though the overall density difference across the salt-stratified fluid layer is stable.[6] Since the difference in thermal and species diffusivities of the binary fluid is responsible for triggering and/or governing convective motion in double-diffusive natural convection systems, it may be anticipated that similar effects can influence convective motion, as well as heat and mass transfer, in systems driven by surface tension forces (Marangoni convection).

As a result of the relevance of double-diffusive Marangoni convection in various crystal growth techniques,[7,8] several studies of Marangoni convection driven by simultaneous temperature and species concentration gradients have been made. A stability analysis has been performed[9] to identify key features associated with the onset of convection. The effect of a surface contaminant on thermally induced Marangoni convection has also been considered.[10] However, additional features of the double-diffusive Marangoni system have not been identified. For example, details of the convective motion within the binary fluid have not been presented in the previous studies. Temperature and concentration distributions within the fluid have not been reported. Evaluation of heat and mass transfer rates has not been considered. Most importantly, perhaps, an investigation of systems that may be incorrectly considered to be nonconvecting but, in fact, undergo convection as a result of double-diffusive effects, has not been made. As such, the objective of the present study is to investigate double-diffusive Marangoni convection in binary fluid systems. Emphasis will be given to systems where diffusional effects can trigger steady convection within the fluid.

It should be noted that, in general, buoyancy and Marangoni driven convection will occur simultaneously when experiments are performed in a gravitational environment. To focus on Marangoni-induced effects that are not influenced by buoyancy, experiments must be performed in drop towers[11] or in space orbit.[12] Because of the relative difficulty in performing gravitationless experimentation, investigation of double-diffusive Marangoni effects will be made with appropriate analytical techniques.

II. ANALYSIS

The system under consideration is shown in Fig. 1. A binary fluid is contained within a two-dimensional cavity of length L, with a free surface at $y = H$. The boundary conditions are associated with end walls maintained at T_1, C_1, and T_2, C_2, respectively. The top surface and bottom wall are adiabatic and impermeable. Buoyancy forces are not considered in the analysis.

With the prescribed boundary conditions, fluid motion is driven by surface tension gradients resulting from simultaneous temperature and species concentration diffusion along the free surface. The two driving forces may, in general, augment or counteract each other. However, to retain the analogy with double-diffusive natural convection, only consideration of the counteracting case will be made. As such, $T_1 > T_2$ and $C_1 < C_2$ for most binary fluids composed of water-soluble organic compounds.[13]

To simplify the analysis and focus attention on the important effects, certain assumptions have been made. First, the free surface of the liquid has been assumed to be flat, that is, the free-surface capillary number is approximately zero.[10] Second, with the exception of surface tension, the thermophysical properties of the liquid have been assumed to be

 0031-9171/86/072103-06$01.90

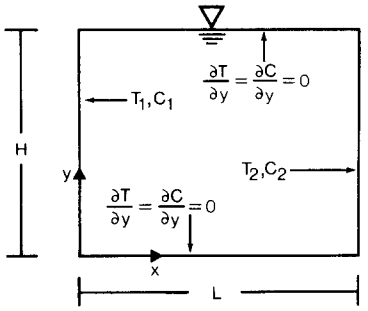

FIG. 1. Schematic of the physical system.

constant. The surface tension is allowed to vary linearly with the liquid temperature and species concentration. Finally, the flow has been assumed to be laminar, and the Soret effect (species transfer resulting from thermal gradients), Dufour effect (heat transfer resulting from species gradients), and viscous dissipation have been neglected.

Subject to these assumptions, the governing equations for the system are the following:

continuity

$$\frac{\partial}{\partial x}(\rho u) + \frac{\partial}{\partial y}(\rho v) = 0, \tag{1}$$

x momentum

$$\frac{\partial}{\partial x}(\rho uu) + \frac{\partial}{\partial y}(\rho uv) = \frac{\partial}{\partial x}\left(\mu \frac{\partial u}{\partial x}\right) + \frac{\partial}{\partial y}\left(\mu \frac{\partial u}{\partial y}\right) - \frac{\partial P}{\partial x}, \tag{2}$$

y momentum

$$\frac{\partial}{\partial x}(\rho uv) + \frac{\partial}{\partial y}(\rho vv) = \frac{\partial}{\partial x}\left(\mu \frac{\partial v}{\partial x}\right) + \frac{\partial}{\partial y}\left(\mu \frac{\partial v}{\partial y}\right) - \frac{\partial P}{\partial y}, \tag{3}$$

energy

$$\frac{\partial}{\partial x}(\rho uT) + \frac{\partial}{\partial y}(\rho vT) = \frac{\partial}{\partial x}\left(\frac{k}{c_p}\frac{\partial T}{\partial x}\right) + \frac{\partial}{\partial y}\left(\frac{k}{c_p}\frac{\partial T}{\partial y}\right), \tag{4}$$

and species concentration

$$\frac{\partial}{\partial x}(\rho uC) + \frac{\partial}{\partial y}(\rho vC) = \frac{\partial}{\partial x}\left(\rho D \frac{\partial C}{\partial x}\right) + \frac{\partial}{\partial y}\left(\rho D \frac{\partial C}{\partial y}\right). \tag{5}$$

The x and y velocities are denoted as u and v. The fluid density, dynamic viscosity, thermal conductivity, specific heat, pressure, and binary diffusion coefficient are ρ, μ, k, c_p, P, and D, respectively. Fluid temperature T and species concentration C are described by Eqs. (4) and (5).

Hydrodynamic boundary conditions include the no-slip requirement for u and v at the bottom of the cavity and v at the cavity end walls.

In general, finite horizontal velocities will exist at the cavity walls resulting from mass transfer across the fluid layer, and may be expressed as[14]

$$u = \frac{-D\,\partial C/\partial x}{(1-C)}. \tag{6}$$

In the present analysis, it is assumed that the binary diffusion coefficient and concentration gradients at the walls are small so that the horizontal velocity described by Eq. (6) may be neglected. As such, the no-slip boundary conditions

$$u = v = 0|_{x=0, x=L, y=0} \tag{7}$$

apply everywhere except at the free surface, where surface tension gradients depend on local temperature and species concentration gradients and induce an effective shear stress expressed as[15]

$$\mu \left.\frac{\partial u}{\partial y}\right|_{y=H} = \left.\frac{\partial \sigma}{\partial T}\right|_C \left.\frac{\partial T}{\partial x}\right|_{y=H} + \left.\frac{\partial \sigma}{\partial C}\right|_T \left.\frac{\partial C}{\partial x}\right|_{y=H}, \tag{8}$$

where σ is the surface tension of the fluid.

The hydrodynamic boundary condition for the y velocity component at the free surface is

$$v|_{y=H} = 0. \tag{9}$$

The thermal and concentration boundary conditions are

$$T = T_1|_{x=0}, \quad T = T_2|_{x=L}, \tag{10}$$

$$\left.\frac{\partial T}{\partial y} = 0\right|_{y=0,\, y=H}, \tag{11}$$

$$C = C_1|_{x=0}, \quad C = C_2|_{x=L}, \tag{12}$$

$$\left.\frac{\partial C}{\partial y} = 0\right|_{y=0,\, y=H}. \tag{13}$$

The governing equations and boundary conditions may be nondimensionalized to identify the dimensionless parameters of the problem. Lengths, velocities, temperature differences, and concentration differences are scaled by L, (α/L), $(T_2 - T_1)$, and $(C_2 - C_1)$ respectively. The thermal diffusivity α is defined as $k/\rho c_p$. Introduction of these scaling variables into the governing equations and boundary conditions yields the following dimensionless parameters:

Prandtl number,

$$\mathrm{Pr} = \nu/\alpha, \tag{14}$$

Lewis number,

$$\mathrm{Le} = \alpha/D, \tag{15}$$

thermal Marangoni number,

$$\mathrm{Ma}_T = \left.\frac{\partial \sigma}{\partial T}\right|_C \Delta T\, L/\mu\alpha, \tag{16}$$

species Marangoni number,

$$\mathrm{Ma}_C = \left.\frac{\partial \sigma}{\partial C}\right|_T \Delta C\, L/\mu\alpha, \tag{17}$$

and the cavity aspect ratio, H/L. The overall Marangoni number may be expressed as

$$\mathrm{Ma} = \mathrm{Ma}_T + \mathrm{Ma}_C \tag{18}$$

and is a measure of the relative strengths of surface tension and viscous forces. Since this study is concerned with double-diffusive Marangoni convection, the ratio of thermally-induced surface tension forces to concentration-induced surface tension forces is useful to consider, and is described by

$$R_\sigma = \frac{\partial\sigma/\partial T|_C\, \Delta T}{\partial\sigma/\partial C|_T\, \Delta C}. \tag{19}$$

The surface tension ratio is analogous to the density ratio, R_ρ, which is used to describe certain aspects of double-diffusive natural convection.[2] At the critical value of the surface tension ratio ($R_\sigma = -1$), thermal Marangoni effects offset species Marangoni effects along the free surface. A trivial solution of the governing equations, in this case, corresponds to stagnant conditions with $u = v = 0$ everywhere.

III. SOLUTION

Solutions of the governing equations were obtained numerically by employing a steady-state version of the SIMPLER algorithm.[16] A 24×24, geometrically spaced computational grid was used to provide fine grid spacing near the walls and top surface of the cavity. The size of the finite difference control volumes was decreased by 10% as y and x (for $x > L/2$) were increased. The solution technique was verified by comparing the predicted heat transfer across a square, air-filled enclosure with differentially heated end walls to a benchmark numerical solution.[17] Values of the overall Nusselt number predicted by the SIMPLER algorithm were within 2% of the benchmark values up to a Rayleigh number of 10^5. Computations were performed for an aspect ratio of 0.5 to amplify Marangoni effects.

IV. RESULTS

Variations in flow patterns, as well as temperature and species concentration distributions, can occur as thermal and species Marangoni effects interact. Figure 2 includes predicted streamlines, isotherms, and isoconcentration lines for $\mathrm{Ma}_T = 1000$, $\mathrm{Le} = 100$, and $\mathrm{Pr} = 5$. The dimensionless temperature Θ is defined as

$$\Theta = (T - T_1)/(T_2 - T_1), \tag{20}$$

while the dimensionless species concentration is

$$\gamma = (C - C_1)/(C_2 - C_1). \tag{21}$$

The dimensionless stream function is calculated from

$$\psi(x,y=0) = \psi(x=0,y=0) - \frac{1}{\nu}\int_0^x v\,dx, \tag{22}$$

$$\psi(x,y) = \psi(x,y=0) + \frac{1}{\nu}\int_0^y u\,dy, \tag{23}$$

with $\psi(x=0,y=0)$ set to zero.

The left panel of Fig. 2 shows predicted quantities of interest for the critical surface tension ratio, $R_\sigma = -1$. The right panel shows behavior of the same system, except the species contribution to the surface tension gradient is ignored, that is, $R_\sigma = -\infty$.

As evident in Figs. 2(a)–2(c), stagnant conditions do not exist. Rather, convective conditions are similar to those which occur for $R_\sigma = -\infty$ [Figs. 2(d)–2(f)]. The most discernible difference between Figs. 2(a)–2(c) and Figs. 2(d)–2(f) is the existence of a small, counter-rotating cell in the upper left corner of the system. The small cell is driven by the surface species concentration gradient at this location. Although relatively large concentration gradients also exist in the upper right corner [Fig. 2(c)], the temperature distribution [Fig. 2(b)] indicates an offsetting, large thermal gradient at this location.

A consequence of the secondary convection cell is the redistribution of the concentration profiles in the upper left corner of Fig. 2(c). An analogous redistribution of the temperature profile is not as pronounced [Fig. 2(b)] as a result

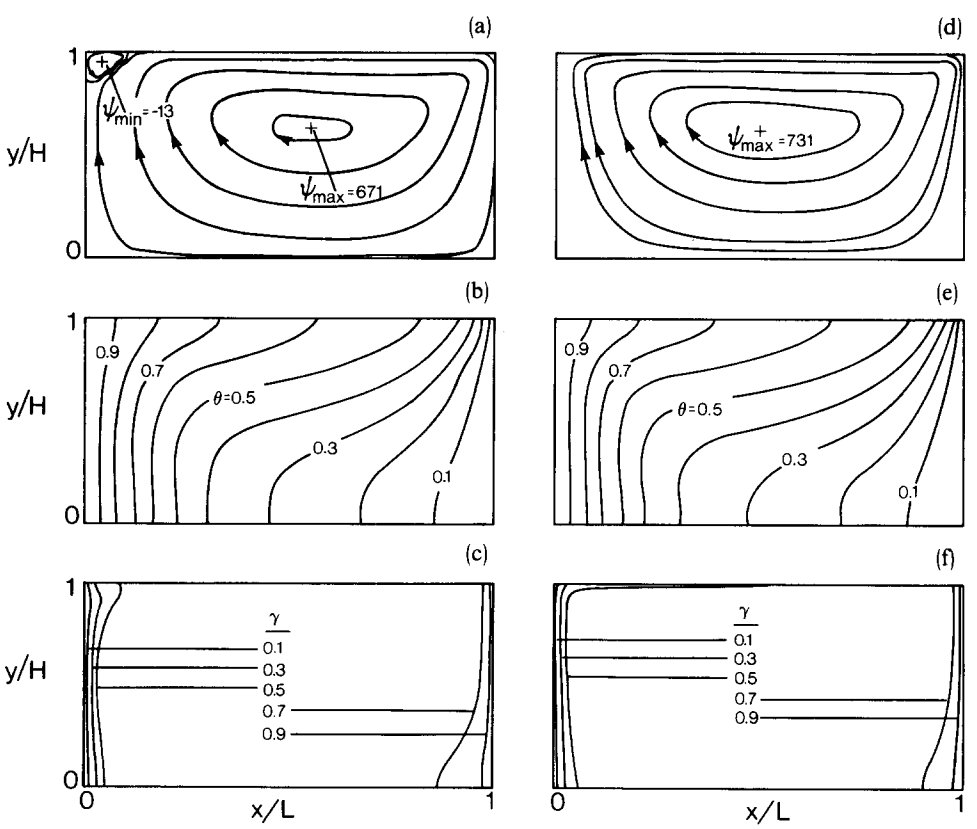

FIG. 2. Predicted streamlines (a),(d), isotherms (b),(e) and isoconcentration lines (c),(f) for $\mathrm{Ma}_T = 1000$, $\mathrm{Le} = 100$, and $\mathrm{Pr} = 5$. Results are for $R_\sigma = -1$ (left) and $R_\sigma = -\infty$ (right).

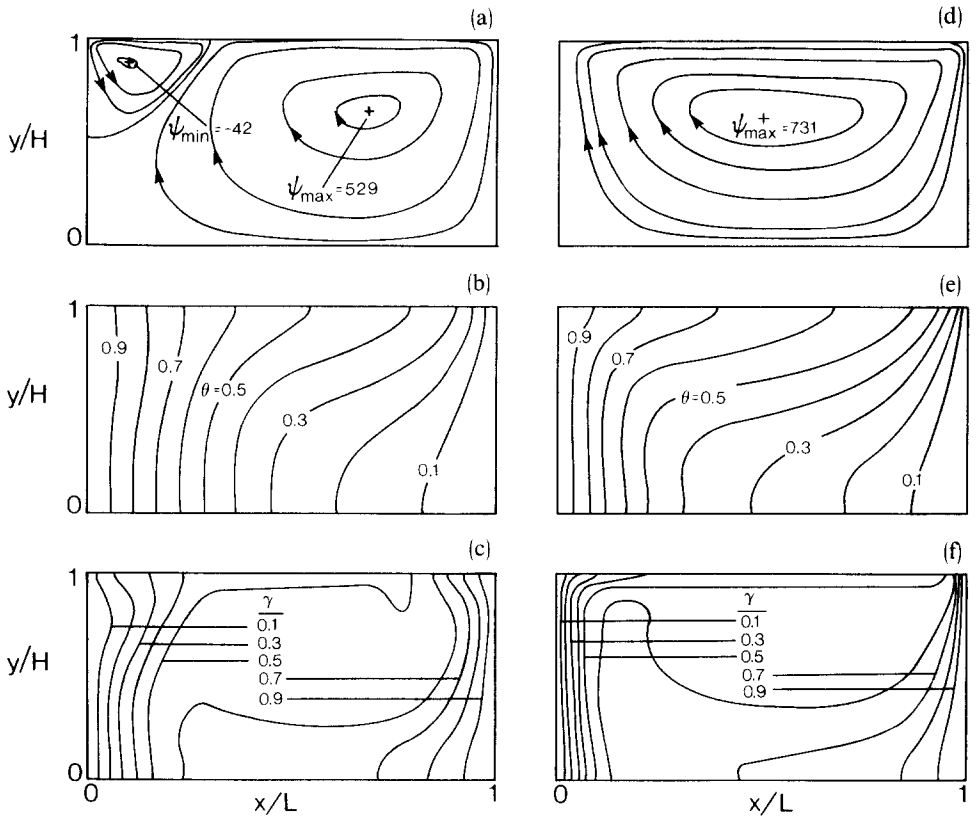

FIG. 3. Predicted streamlines (a),(d), isotherms (b),(e) and isoconcentration lines (c),(f), for $Ma_T = 1000$, $Le = 10$, and $Pr = 5$. Results are for $R_\sigma = -1$ (left) and $R_\sigma = -\infty$ (right).

of the large Le associated with the conditions of Fig. 2.

As the Lewis number of the binary fluid is decreased, species diffusion will become more influential. In fact, as Le approaches unity, stagnant conditions are predicted to occur, if $R_\sigma = -1$. It is of interest, therefore, to examine how the results of Fig. 2 vary as Le becomes smaller. Figure 3 shows predicted streamlines, isotherms, and isoconcentration lines for $Ma_T = 1000$, $Le = 10$, and $Pr = 5$. The left panel of Fig. 3 includes results for $R_\sigma = -1$ while the right panel is associated with $R_\sigma = -\infty$.

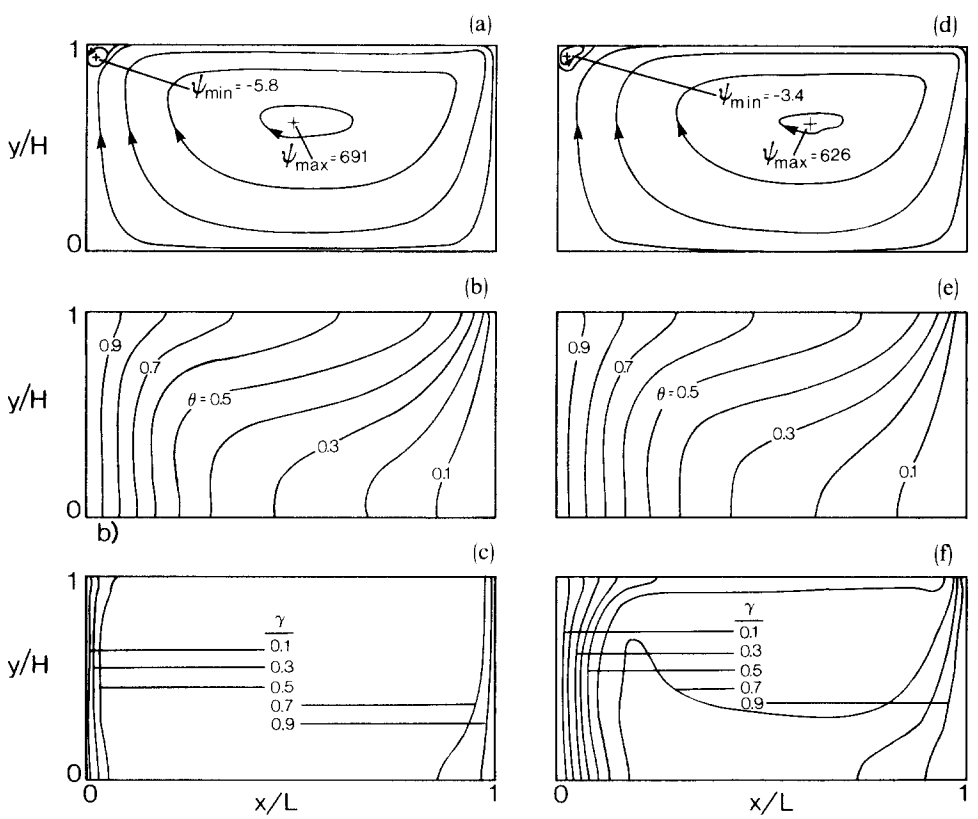

FIG. 4. Predicted streamlines (a) and (d), isotherms (b) and (e) and isoconcentration lines (c) and (f) for $Ma_T = 1000$, $R_\infty = -2$, and $Pr = 5$. Results are for $Le = 100$ (left) and $Le = 10$ (right).

A comparison of Fig. 3(a) with Fig. 2(a) indicates that the species-induced, counter-rotating cell at $x = 0$, $y = H$ becomes larger and rotates at greater speed as Le decreases. Whereas the concentration profiles were moderately displaced by double-diffusive Marangoni effects in Fig. 2(c), they are more noticeably displaced in Fig. 3(c). Because the Lewis number is smaller in Fig. 3 than in Fig. 2, the temperature distributions in the upper left corner also indicate a moderate displacement [Figs. 2(b) and 2(e)].

The results of Figs. 2 and 3 show that species diffusion can affect flow conditions in systems which may be incorrectly assumed to be stagnant. If species contributions to the surface tension gradient at $y = H$ are ignored, the resulting behavior bears similarity to the double-diffusive system when $R_\sigma = -1$.

In most systems $R_\sigma \neq -1$. It is of interest, therefore, to examine predicted system behavior for cases where the overall surface tension difference across the free surface is nonzero. Figure 4 includes predicted behavior when thermally induced surface tension effects are twice as influential as species induced effects, that is, $R_\sigma = -2$. The predictions correspond to $\mathrm{Ma}_T = 1000$ and $\mathrm{Pr} = 5$. The left panel is associated with $\mathrm{Le} = 100$ and the right panel with $\mathrm{Le} = 10$.

Streamline [Figs. 4(a) and 4(d)] and isotherm [Figs. 4(b) and 4(e)] distributions are similar. A small counter-rotating cell is located in the upper left corner, regardless of the value of Le. The larger, thermally driven cell occupies most of the system. Differences in the temperature distributions cannot be distinguished, although the concentration distributions [Figs. 4(c) and 4(f)] vary as a result of the difference in thermal and species diffusion rates. As such, species diffusion effects on convection become less pronounced with increasing R_σ.

In many systems, for example those associated with crystal growth,[7,8] convective conditions within the bulk fluid are important, in that they govern local heat and mass transfer at a solid–liquid interface. In all of the situations considered so far, a secondary convection cell develops at the upper left boundary as a result of double-diffusive Marangoni effects. It may be expected, therefore, that local heat and mass transfer rates vary significantly, even though convection within the bulk fluid is not radically altered by species diffusion.

The local Nusselt and Sherwood numbers are a measure of the dimensionless heat and mass transfer rates and are defined as[14]

$$\mathrm{Nu} = hL/k, \quad \mathrm{Sh} = h_m L/D \tag{24}$$

where the local heat and mass transfer coefficients, h and h_m, are expressed as

$$h = \frac{|k\,\partial T/\partial x|}{(T_2 - T_1)}, \quad h_m = \frac{|D\,\partial C/\partial x|}{(C_2 - C_1)}. \tag{25}$$

The Nu and Sh distributions along $x = 0$ are presented for $\mathrm{Ma}_T = 1000$, $\mathrm{Le} = 100$, and $\mathrm{Pr} = 5$ in Fig. 5.

Although the counter-rotating cells of Figs. 2(a) and 4(a) are small and do not greatly affect the larger, thermally driven convection cell, local mass transfer (Sh) is significantly altered. This effect is most pronounced at $y/H \simeq 0.85$ and corresponds to decreased local mass transfer, as fluid of

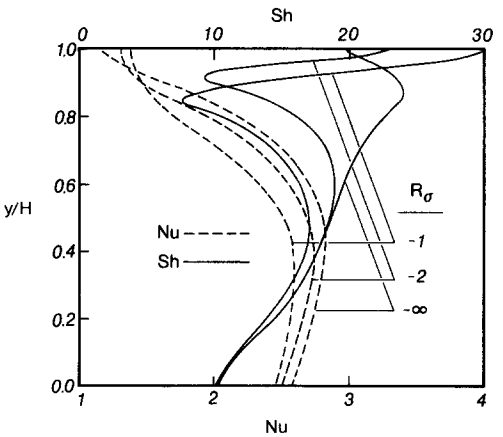

FIG. 5. Local Nusselt and Sherwood distributions at $x = 0$ for $\mathrm{Ma}_T = 1000$, $\mathrm{Le} = 100$, and $\mathrm{Pr} = 5$.

relatively small γ is collected at the boundary between the two convection cells. As expected, surface tension effects are less pronounced at small y/H. These results show that double-diffusive Marangoni phenomena should be considered in systems where local mass transfer determination, or control, is important.

As a result of the large Le associated with Fig. 5, local heat transfer variations are not as pronounced as the mass transfer variations and the qualitative shape of the Nu distribution is retained, regardless of R_σ. In general, a slightly smaller Nu occurs along $x = 0$ as a result of decreased rotational speed of the large convection cell [Figs. 2(a), 2(d), and 4(a)] associated with decreasing absolute values of R_σ.

The local mass transfer variation evident in Fig. 5 may lead to a change in the total heat and mass transfer across the fluid layer. As such, the average (overall) Nusselt and Sherwood numbers defined as

$$\overline{\mathrm{Nu}} = \frac{1}{H}\int_{y=0}^{H} \mathrm{Nu}\,dy, \quad \overline{\mathrm{Sh}} = \frac{1}{H}\int_{y=0}^{H} \mathrm{Sh}\,dy, \tag{26}$$

respectively, will depend on double-diffusive Marangoni effects. The extent of this dependence is shown in Fig. 6 with $\overline{\mathrm{Nu}}$ and $\overline{\mathrm{Sh}}$ plotted against Le and R_σ. The thermal Marangoni number is 1000 while $\mathrm{Pr} = 5$.

When species contributions to the surface tension gradient are neglected ($R_\sigma = -\infty$), maximum heat and mass transfer rates occur. Since the flow field is independent of the

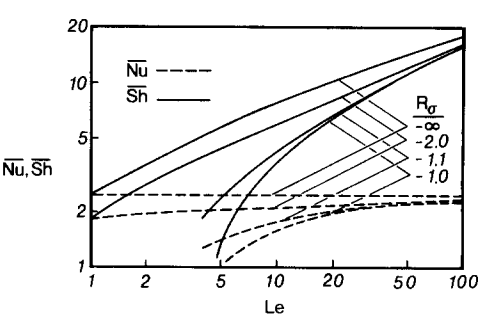

FIG. 6. Average Nusselt and Sherwood numbers versus Le and R_σ.

species concentration, $\overline{Nu}$ is constant. Overall Sherwood numbers vary from 2.48 at Le = 1 to approximately 18 at Le = 100.

As the counter-rotating cell is established by double-diffusive Marangoni considerations, smaller $\overline{Nu}$ and $\overline{Sh}$ occur for all Le. However, as Le increases, $\overline{Nu}$ and $\overline{Sh}$ approach the $R_\sigma = -\infty$ limiting values. These results are consistent with the qualitative observations of the flow conditions shown in Figs. 2–4.

Perhaps the most interesting behavior illustrated in Fig. 6 is that associated with $R_\sigma = -1.1$ and -1.0 near Le = 5. Both $\overline{Nu}$ and $\overline{Sh}$ decrease rapidly as Le is decreased. This result suggests that stagnant conditions occur at small, nonzero Le for small absolute values R_σ. Hence, a critical Le may exist for a system characterized by a given aspect ratio, Ma_T, R_σ, and Pr, below which stagnant, fluid conditions occur.

V. CONCLUSIONS

The present study has investigated double-diffusive Marangoni convection. Results indicate that convection may occur, even though the overall Marangoni number is zero. The convection pattern consists of a secondary counter-rotating cell in the upper corner of the system and can lead to variations in local and overall heat and mass transfer rates.

Certain details of system behavior associated with double-diffusive Marangoni convection effects have been illustrated. The study is, by no means, complete since many questions remain unanswered. For example, system behavior associated with fluids of different Pr is not known. Systems characterized by a different geometry may be influenced by double-diffusive Marangoni convection to a different extent. Convective behavior may also vary with the sign of $\partial\sigma/\partial C$, since the concentration boundary conditions would need to be reversed to produce double-diffusive phenomena. Behavior for systems characterized by $|R_\sigma| < 1$ is also unknown. Finally, the interaction of double-diffusive Marangoni and natural convection has not been addressed. Consideration of these and other problems may be made in future analyses.

ACKNOWLEDGMENTS

Appreciation is extended to Professor Satish Ramadhyani of Purdue University for helpful discussions concerning implementation of the numerical algorithm. Computational facilities were provided by the Computation Center and the Department of Mechanical Engineering at the University of Texas at Austin.

Support of this work by the National Science Foundation under Grant No. CBT-8552806 is gratefully acknowledged.

[1] S. Ostrach, Adv. Heat Transfer **7**, 161 (1972).
[2] J. S. Turner, *Buoyancy Effects in Fluids* (Cambridge U.P., Cambridge, England, 1979).
[3] C. S. Yih, Phys. Fluids **11**, 477 (1968).
[4] V. Stanek and J. Szekely, Chem. Eng. Sci. **25**, 699 (1970).
[5] H. E. Huppert and P. F. Linden, J. Fluid Mech. **95**, 431 (1979).
[6] T. L. Bergman, F. P. Incropera, and R. Viskanta, Int. J. Heat Mass Transfer **28**, 779 (1985).
[7] D. Schwabe, Physicochem. Hydrodyn. **2**, 263 (1981).
[8] S. Ostrach, Trans. ASME J. Fluids Eng. **105**, 5 (1983).
[9] C. L. McTaggert, J. Fluid Mech. **134**, 301 (1983).
[10] G. M. Homsy and E. Meiburg, J. Fluid Mech. **139**, 443 (1984).
[11] S. Ostrach and A. Pradhan, AIAA J. **16**, 419 (1978).
[12] R. Monti and G. Mannera, Acta. Astron. **12**, 511 (1985).
[13] A. M. Scwartz and J. W. Perry, *Surface Active Agents* (Interscience, New York, 1966).
[14] F. P. Incropera and D. P. DeWitt, *Fundamentals of Heat and Mass Transfer* (Wiley, New York, 1985).
[15] V. G. Levich and V. S. Krylov, Ann. Rev. Fluid Mech. **1**, 293 (1969).
[16] S. V. Patankar, *Numerical Heat Transfer and Fluid Flow* (McGraw-Hill, New York, 1980).
[17] G. E. de Vahl Davis, Int. J. Num. Meth. Fluids **3**, 249 (1983).